



Effect of streak employing control of oblique-breakdown in a supersonic boundary layer with weak wall heating/cooling

M. Celep , A. Hadjadj, and M. S. Shadloo *

CORIA-UMR 6614, CNRS-University, INSA of Rouen and Normandie University, 76000 Rouen, France

S. Sharma

Johnson & Johnson (JJSBF), Campus de Maigremont, 27100 Val-de-Reuil, France

M. Yildiz

Integrated Manufacturing Technologies Research and Application Center & Faculty of Engineering and Natural Sciences, Sabanci University, Orhanli, Tuzla, Istanbul 34956, Turkey

M. J. Kloker 

Institute of Aerodynamics and Gas Dynamics, University of Stuttgart, 70550 Stuttgart, Germany



(Received 19 December 2021; accepted 27 April 2022; published 31 May 2022)

Contrary to incompressible flows, there has been an immense research gap in the flow transition control using velocity streaks for supersonic flows. The first direct numerical simulations (DNS) study in this direction was conducted at Mach 2.0 for an adiabatic wall condition and showed that effective control could be provided by employing streak modes having four to five times the fundamental wave number of the most amplified oblique disturbance waves. However, the application range of the method in terms of the control amplitude is studied roughly and only for adiabatic walls. The present study scrutinizes the controlling capability of these decaying streak modes under the influence of both adiabatic and weak wall heating/cooling by means of DNS. The stabilizing/destabilizing influence of the control streaks in combination with different thermal boundary conditions in a perturbed boundary layer is shown. The effective range of the streak amplitudes under the given flow conditions is presented both for adiabatic and isothermal wall conditions. No significant impact of the wall-boundary condition on the control-streak development is observed in the sustainable flow control range, but the useful control-streak amplitude range diminishes with wall heating.

DOI: [10.1103/PhysRevFluids.7.053904](https://doi.org/10.1103/PhysRevFluids.7.053904)

I. INTRODUCTION

Increasing attention on emission reduction and designing an economically sustainable supersonic aircraft are just a few reasons among many others that augmented the interest in understanding the laminar-to-turbulent flow transition. Keeping the flow laminar as much as possible has been the primary intention to decrease the skin friction around the aerodynamic vehicle in order to reduce the drag which naturally decreases the fuel consumption and thermal load on the body. However, transition might also be desired in the case of scramjet applications where the boundary layer is tripped deliberately to have a uniform turbulent flow at the entrance of the combustor inlet [1]. For

*msshadloo@coria.fr

all these reasons, it is highly important to have a better comprehension and a possible control of the transition phenomenon, which ultimately requires further elaboration of its governing mechanism.

For incompressible flows, the flow transition in a low-disturbance environment is driven by two-dimensional (2D) sinusoidal waves, called Tollmien-Schlichting (TS). Moving further downstream, these waves are superseded by the secondary instability mechanism, corresponding to the weakly nonlinear stage in the roadmap of Fedorov [2] with the appearance of Λ -shaped vortices [3,4] located near the boundary-layer edge. Their breakdown forms turbulent spots which coalesce to generate turbulence as the flow moves downstream. However, in compressible flows, the most-amplified waves become three-dimensional running obliquely with respect to the free-stream with a nonzero inclination angle. For a transonic boundary layer at Mach number 1.6, direct numerical simulations (DNS) studies of Thumm [5] and Fasel *et al.* [6] were the first illustrating that the transition is controlled by oblique breakdown which is initiated by a pair of most-amplified waves traveling at identical but opposite wave angles with respect to the free-stream. Once emerged, the self-nonlinear interaction of these waves generates the steady vortex mode (0,2) in the domain, thus closing the wave-vortex triad [7]. Moving downstream in the flow, higher harmonic modes are generated by the interaction of the most-amplified disturbance and the steady mode resulting in a broader frequency/wave-number spectrum extending the energy exchange mechanism to a more complex stage [8]. Furthermore, a study of Fezer and Kloker [9] unraveled the predominant effect of the fundamental mode than three-dimensional subharmonic modes in terms of growth rates, although the transition process is found to be accelerated by the presence of subharmonic waves. The DNS study of Husmeier *et al.* [10] for various breakdown scenarios at Mach = 3 proved that the oblique breakdown scenario is the most viable path to that transition. For an overall understanding of the oblique breakdown mechanism in two-dimensional supersonic flows, the reader is referred to Mayer *et al.* [11]. Since then, oblique breakdown triggered by the unsteady 3D mode has been proven to be the most dominant mechanism in flow transition of supersonic flows for a wide range of Mach numbers over flat surfaces. In a more realistic situation, natural transition scenario, the interaction between waves should be considered rather than perturbing the flow solely by one single pair of waves. Laible *et al.* [12] concluded that multiple pairs of waves may result in earlier breakdown with a shorter transitional region than the case with a single pair of waves, also verified by Chang and Malik [7] over flat-plates. To elaborate on the feeding mechanism of disturbance modes, temporal DNS was used for simulating an oblique breakdown over a flat plate. It was revealed that the modes (0,0), (2,2), (2,0) are generated only through the self-nonlinear interaction of the fundamental disturbance and remain completely unaffected by their linear eigenbehavior. Steady longitudinal mode (0,2), on the other hand, exhibits transient growth after having generated by the primary mode [12].

Regarding the transition control in incompressible flows, closely spaced streak vortices, i.e., those carrying higher wave number than the most-amplified mode are found effective in postponing the transition onset by dampening the most-amplified cross-flow vortices over an infinite swept wing [13]. The use of these vortical structures was extended to a flat-plate configuration where TS waves dominate the transition mechanism in a low-disturbance environment. Vortex-induced streamwise streaks bearing sufficiently large amplitude are capable of delaying transition by surpassing these two-dimensional waves while early transition might be triggered above some critical amplitude [14]. This phenomenon was later verified experimentally by Fransson *et al.* [15,16] in which a series of roughness elements placed in the spanwise direction to generate streaks of moderate amplitudes. Furthermore, stabilizing effect of finite-amplitude streaks on the linear amplification of unstable perturbations, TS, and oblique waves, was investigated by means of nonlinear parabolized-stability-equations (PSE). A careful examination revealed the existence of an optimum spanwise wave number for diminishing the growing perturbation [17]. Alternative methods such as miniature vortex generators [18] and plasma actuators [19] were also used to generate streamwisely elongated streaks and highlight their stabilizing influence in low-speed boundary layers. However, the stabilizing effect of the streaks in supersonic flows was studied only quite recently by Paredes *et al.* [20]. Their analysis of the steady growing streaks with the use of nonlinear plane-marching PSE showed

that streaks are required to carry a wave number at least two times the one of the fundamental disturbance, i.e., first-mode oblique wave. It was also revealed that mean-flow-deformation (MFD) is in favor of stabilizing the first mode. Direct nonlinear control of oblique breakdown has been investigated by Sharma *et al.* [21] in a comprehensive DNS study in a supersonic boundary layer at $M_\infty = 2.0$, with the use of streamwisely elongated streak structures forced by a blowing-and-suction strip. A blowing/suction strip placed at the wall is employed to generate these vortices, decaying in the streamwise direction, in their study over a flat-plate with adiabatic wall condition. Consequently, streak modes having four to five times the fundamental wave number are found to be effective in controlling the transition. However, it is pointed out that maximum streak amplitude higher than about 25% of $\rho_\infty u_\infty$ results in early transition due to strong streak-mode instability. Here “ ∞ ” refers to the free-stream conditions. Moreover, the MFD and 3D part of the control are found responsible of the stabilizing effect by reducing the growth of the most amplified instability mode. Their findings concerning the MFD conforms with those of Paredes *et al.* [20], whereas it was indicated that the 3D part of the control requires the spanwise wavelength to be smaller by about 2.5 times the local boundary-layer thickness. Later, Kneer *et al.* [22] applied an identical control technique to a scenario that includes subharmonic modes which were previously found to be accelerating the flow transition with the fundamental mode [9]. In their preceding study [23], the impact of relatively moderate wall cooling on the downstream development of the control streaks and their controlling capabilities were investigated for an isothermal wall at $T_w = 0.9 \times T_{ad}$, where T_w and T_{ad} are wall and adiabatic temperatures for laminar flow, respectively. According to linear stability theory (LST) [24,25], cooling alone stabilizes the first mode disturbances, whereas its effect is reversed for the second mode (Mack mode) which is intrinsically neglected given the low free-stream Mach number in the concerning study. The introduction of the control streaks with wall cooling further delayed the flow transition by reducing the growth of the fundamental mode (1,1) and the inherent streaky mode (0,2) in oblique breakdown. However, no significant effect was remarked on the downstream development of the control mode and the hampering role of the MFD.

Although, the pioneering DNS studies [21–23] had laid out to a good amount of knowledge concerning the streak employing transition control, there still remains some open questions that will be addressed in this study. For instance, what is the range of streak amplitudes that is successful in suppressing the flow transition for both adiabatic and isothermal wall conditions? Besides, does heating have a significant impact on the downstream development of the control streaks? To the best knowledge of the authors, the heated scenario has not been reported in the literature so far. In the present work, contrary to Kneer [23] where a new pair of most-amplified disturbance, estimated by LST, is used for the cooled scenario, the identical fundamental mode of the adiabatic case is retained here for both heated and cooled walls. Given the low amount of heating/cooling (5%) whose effect on LST results might be considered negligible, the examination of the effects of pure isothermal wall condition becomes viable.

The paper is organized as follows. Section II provides details about the computation setup including the used DNS solver, boundary conditions, and flow-geometry configuration of interest. Thereafter, the results starting with the effective control scenario under various thermal wall boundary conditions are provided in Sec. III. Following the parametric study of the control amplitude in Sec. III C, the conclusion is made in Sec. IV.

II. COMPUTATION SETUP

A. Numerical solver

The present study utilizes an in-house developed direct numerical-/large eddy simulation numerical solver known as compressible high-order code using Weno adaptive stencils, which solves three-dimensional, compressible, unsteady Navier-Stokes equations for perfect gases. Convective fluxes are discretized by a hybrid conservative fourth-order split centered finite-difference scheme with a fifth-order weighted essential nonoscillatory scheme. Convective terms are split in

skew-symmetric form to minimize the aliasing error and to enforce the discrete conservation of the kinetic energy to achieve numerical stability. The diffusive terms, expressed in compact form, are approximated with a fourth-order scheme. The system of equations is time-integrated using a third-order RungeKutta scheme. The solver has been validated and proven its practicality in various applications [26,27].

B. Governing equations

The Newtonian fluid motion is governed by the Navier-Stokes equations comprising of the equations of conservation of mass, momentum, and total energy. This set of equations is written as follows:

$$\frac{\partial \rho}{\partial t} + \frac{\partial \rho u_j}{\partial x_j} = 0, \quad (1)$$

$$\frac{\partial \rho u_i}{\partial t} + \frac{\partial \rho u_i u_j}{\partial x_j} = -\frac{\partial p}{\partial x_i} + \frac{\partial \tau_{ij}}{\partial x_j}, \quad (2)$$

$$\frac{\partial \rho E}{\partial t} + \frac{\partial (\rho E + p) u_j}{\partial x_j} = -\frac{\partial q_j}{\partial x_j} + \frac{\partial u_i \tau_{ij}}{\partial x_j}, \quad (3)$$

where the pressure is given by:

$$p = (\gamma - 1)(\rho E - \frac{1}{2} \rho u_i u_i), \quad (4)$$

where γ and M denote the heat capacity ratio and Mach number, respectively. τ is the viscous stress tensor, given by:

$$\tau_{ij} = \mu \left(\frac{\partial u_j}{\partial x_i} + \frac{\partial u_i}{\partial x_j} - \frac{2}{3} \frac{\partial u_k}{\partial x_k} \delta_{ij} \right), \quad (5)$$

Here ρ , u , and p represent density, velocity components, and pressure, respectively, whereas δ_{ij} is the Kronecker delta with Re indicating the Reynolds number. The fluid of interest is air, with constant specific heat capacities, whose dynamic viscosity is assumed to be only temperature dependent and calculated by the Sutherland's law,

$$\mu(T) = \frac{C_1 T^{3/2}}{T + S}. \quad (6)$$

Here Sutherland's temperature for air is $S = 110.4$ K and the constant $C_1 = 1.458 \times 10^{-6}$ kg/ms \sqrt{K} which is calculated through $C_1 = \mu_r(T_r + S)/T_r^{3/2}$. Reference dynamic viscosity of air $\mu_r = 1.716 \times 10^{-5}$ kg/ms at the reference temperature, T_r of 273.15 K, where the subscript r refers to the reference values.

C. Problem setup

Simulations are carried out for supersonic flows at Mach number $M_\infty = 2.0$, with temperature $T_\infty = 160$ K, velocity $u_\infty = 507.1$ m/s, kinematic viscosity $\nu_\infty = 2.1067 \times 10^{-5}$ m²/s, pressure $p_\infty = 23.786$ kPa and Prandtl number $Pr = 0.72$. The unit Reynolds number $Re_u = \frac{u_\infty}{\nu_\infty} = 2.407 \times 10^7$ m⁻¹. Here “ ∞ ” denotes the free-stream flow conditions. Following the schematic of the computational domain presented in Fig. 1, the inlet location, $x_{in} = 4.154$ mm, corresponding to the inlet Reynolds number, $Re_{x_{in}} = \frac{u_\infty x_{in}}{\nu_\infty} = 10^5$, is designated far enough from the leading edge to preclude possible interactions between weakly generated shocks at the leading edge and the disturbance modes of the boundary layer. The length and the height of the domain are $L_x = 55$ mm and $L_y = 10.2$ mm, respectively, while the width of the domain corresponds to the fundamental wavelength of the disturbed mode, $L_z = 2.153$ mm. Grid is distributed equidistantly in streamwise, x , and spanwise, z directions with $N_x = 800$ and $N_z = 140$ number of points, while grid stretching

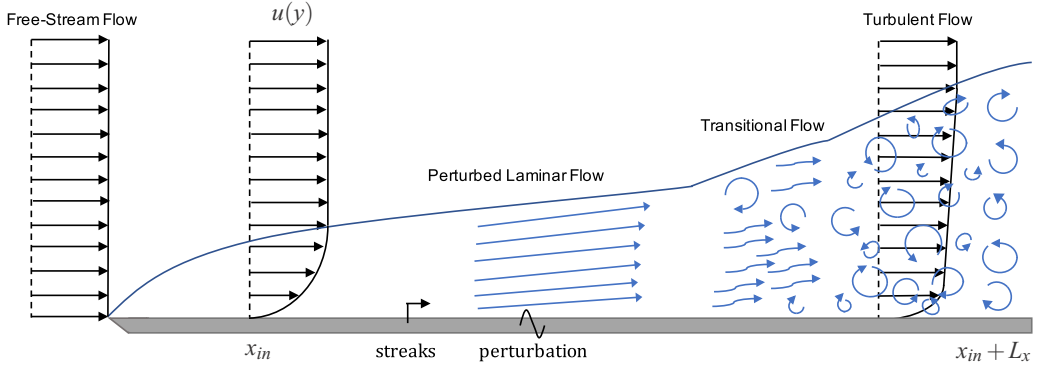


FIG. 1. Schematic of the computational domain and boundary conditions. L_x , x_{in} , $u(y)$ denote the length of the domain, inlet location, and streamwise velocity in the wall-normal direction, respectively.

function is used with $N_y = 180$ in the wall-normal direction for accurately capturing the inner boundary layer next to wall which given as

$$y = L_y \left(1 + \frac{\tanh \kappa y}{\tanh \kappa} \right), \quad (7)$$

where the stretching parameter $\kappa \approx 3$.

D. Boundary conditions

Blowing/suction strips whose formulations are identical as in the case of Sharma *et al.* [21] are used here. The laminar boundary layer is excited via blowing and suction strip extending from $Re_{x_1} = 2 \times 10^5$ to $Re_{x_2} = 3.32 \times 10^5$ and can be expressed as

$$\dot{m}(x, y = 0, z, t) = \rho v = A \rho_\infty u_\infty f(x) g(z) h_1(t), \quad (8)$$

$$f(x) = 4 \sin \theta(x) [1 - \cos \theta(x)] / \sqrt{27}, \quad (9)$$

$$\theta(x) = 2\pi [x - (x_1 - x_{in})] / (x_2 - x_1), \quad (10)$$

$$g(z) = (-1)^k \cos(2\pi k z / L_z), \quad (11)$$

$$h_1(t) = \sin(\omega t), \quad (12)$$

where A is the disturbance amplitude given as $(\rho v)_{wall} / (\rho_\infty u_\infty)$, \dot{m} is the cross-stream mass flux, ω is the angular frequency of the excitation mode, h being the multiple of the fundamental frequency and k the multiple of the fundamental spanwise wave number. Here $A = 3.27 \times 10^{-4}$, the fundamental frequency $f_0 = 73.87$ kHz and wave number $\beta_0 = 2\pi / \lambda_z = 2.9176 \times 10^3 \text{ m}^{-1}$ corresponding to the most amplified modes (1,1) and (1,-1) based on the linear stability theory. Note that (h, k) indicates the disturbance mode with frequency $h \times f_0$ and spanwise wave number $k \times \beta_0$, while it stands for the sum of $(h, +k)$ and $(h, -k)$. Furthermore, an additional strip placed in between $Re_{x_{c,1}} = 1.48 \times 10^5$ to $Re_{x_{c,2}} = 1.96 \times 10^5$, is used to introduce steady control streaks, such as

$$\dot{m}(x, y = 0, z) = \rho v = A_c \rho_\infty u_\infty f(x) g(z), \quad (13)$$

$$f(x) = 2.5983 [1 - \cos \theta(x)] / \sqrt{27}. \quad (14)$$

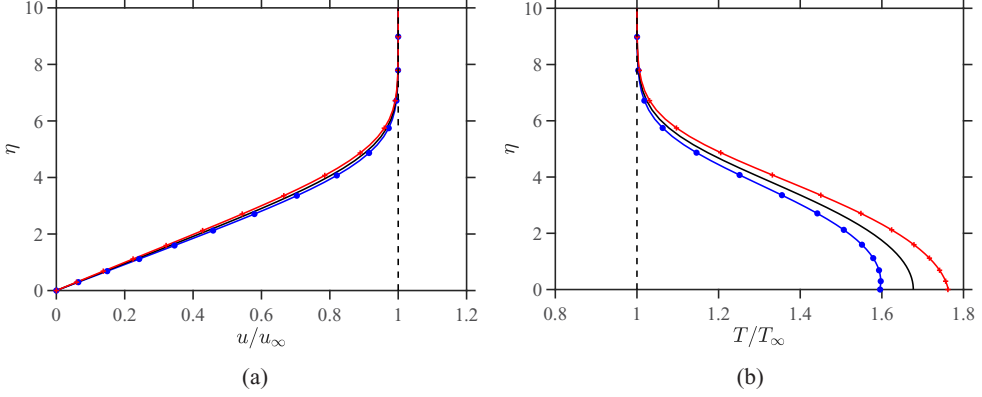


FIG. 2. (a) Velocity and (b) temperature profiles obtained through DNS at $Re_x = 10^5$. Cooled (\bullet), adiabatic ($-$), and heated ($+$) with $\eta = y\sqrt{\frac{u_\infty}{\nu_\infty x}}$.

with a control amplitude $A_c = 1.22 \times 10^{-2}$, while $\theta(x)$ and $g(z)$ formulations of the perturbation strip are retained. It is noted that the mean net mass flux injected to the domain in both of the strips is zero. Supersonic inflow and outflow conditions are applied at the inlet ($x = x_{in}$) and at the outlet ($x = x_{in} + L_x$) of the computational domain, respectively. To obtain the inlet boundary conditions, a different method is performed than the one used by Sharma *et al.* [21]. Self-similarity solution from the compressible boundary-layer equations is obtained at $Re_x = 5 \times 10^4$, which is used at the inlet of a DNS simulation where neither of the strips is activated. Results, collected at $Re_x = 10^5$, based on density, temperature and velocity profiles are used as input for the main simulations. Figure 2 shows the nondimensional velocity and temperature profiles at the inlet for different boundary conditions. It is observed that the deviation between the cases is palpable in the temperature profiles, whereas a minute difference is seen in those of velocities. Besides, the boundary-layer thickness at the inlet is found identical, $\delta_{in} = 8.823 \times 10^{-2}$ mm for all the cases. The reason is attributed to the low rate of heating/cooling and low inlet Reynolds number. As for the rest of the boundaries, periodicity is imposed at the side walls. No-slip condition is applied at the wall with the permeable region occupied by the perturbation and control strips. The wall is assumed to be either adiabatic or fixed temperature, $T_w = 0.95 \times T_{aw}$ for cooled wall, $T_w = 1.05 \times T_{aw}$ for heated wall, where $T_{aw} = T_\infty[1 + \frac{1}{2}(\gamma - 1)Pr^{1/2}M_\infty^2]$. A slip condition with zero boundary-normal gradient is imposed at the upper boundary. In what follows is the analysis of various simulations under different conditions. For simplicity, the details about the performed cases are enlisted in Table I.

TABLE I. Computational parameters for various cases.

Cases	T_w/T_{aw}	Control mode	A_c
A5C	1	(0,5)	1.22×10^{-2}
C5C	0.95	(0,5)	1.22×10^{-2}
H5C	1.05	(0,5)	1.22×10^{-2}
A _T	1	—	0
C _T	0.95	—	0
H _T	1.05	—	0

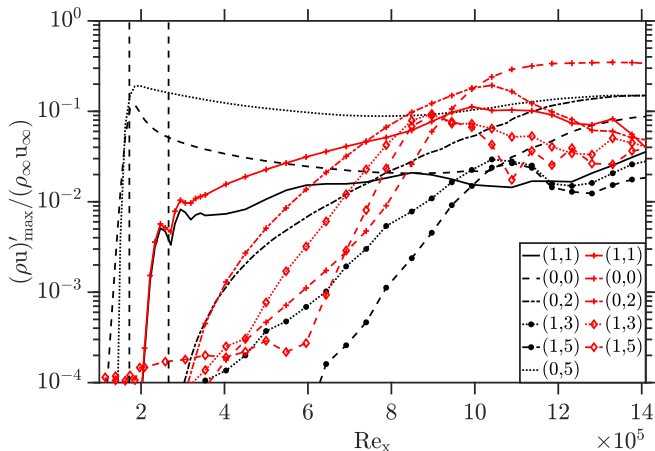


FIG. 3. Streamwise evolution of the maximum disturbance amplitudes of various modes for A_T (+, \diamond) and $A5C$ (—, \bullet). The vertical dashed lines indicate the midpoint of the disturbance and the control strips with respect to streamwise direction.

III. RESULTS AND DISCUSSION

A. Adiabatic wall

The validation of the solver for transitional supersonic boundary layers was already performed by Sharma *et al.* [21]. A comparison was done with the results of Fezer and Kloker [9] in terms of growing modes in the boundary layer and a good collapse of data is presented. Therefore, the current paper starts directly with the efficient use of velocity streaks in delaying the transition. Before embarking on the influence of the isothermal boundary conditions on the control streaks, simulations are performed for adiabatic wall condition. The control mode (0,5) is used in $A5C$, whereas no control is activated in A_T . A comparison between the cases is made in terms of the evolution of the disturbance modes with respect to streamwise direction, see Fig. 3. Hereby, each mode is computed by a time-sampling over two fundamental periods. Fourier transform is performed in time and in the spanwise direction, whose maximum value in the wall-normal direction is plotted. The reader is referred to Sharma [26] and Kloker [28] for more details about the data sampling for disturbance modes. It is inferred from Fig. 3 that the growth rate reduction in the fundamental (1, \pm 1) and the nonlinearly generated steady (0,2) modes illustrates the transition delaying effect of the control streaks. Besides, introducing the control streaks resulted in an earlier generation of MFD (0,0), which plays a vital role in delaying the flow transition [20]. From the physical point of view, MFD can be defined as the distortion from the baseflow, where neither of the strips is activated, as a consequence of introducing disturbance and control modes. In the absence of the control mode (0,5), chaotic nature of turbulence demonstrates itself in the amplitudes of the fundamental disturbance mode (1,1) and nonlinearly generated (1,3), (1,5) 3D unsteady modes at around $Re_x = 9 \times 10^5$. In the meantime, a saturation sets in for the MFD after having reached an amplitude of $\approx 35\%$ of $\rho_\infty u_\infty$, whereas an exponential drop is observed in (0,2). The oscillations in the low-amplitude region attributed to the higher background noise intrinsic in our solver [23]. As a continuation of the work of Sharma *et al.* [21], the current research is aligned in the direction of elaborating the effects of wall cooling/heating on the downstream development of the disturbances in the following section.

B. Isothermal wall

This section is dedicated to the study of the influence of isothermal wall conditions on downstream development of the control streaks and the modulation of various disturbance modes.

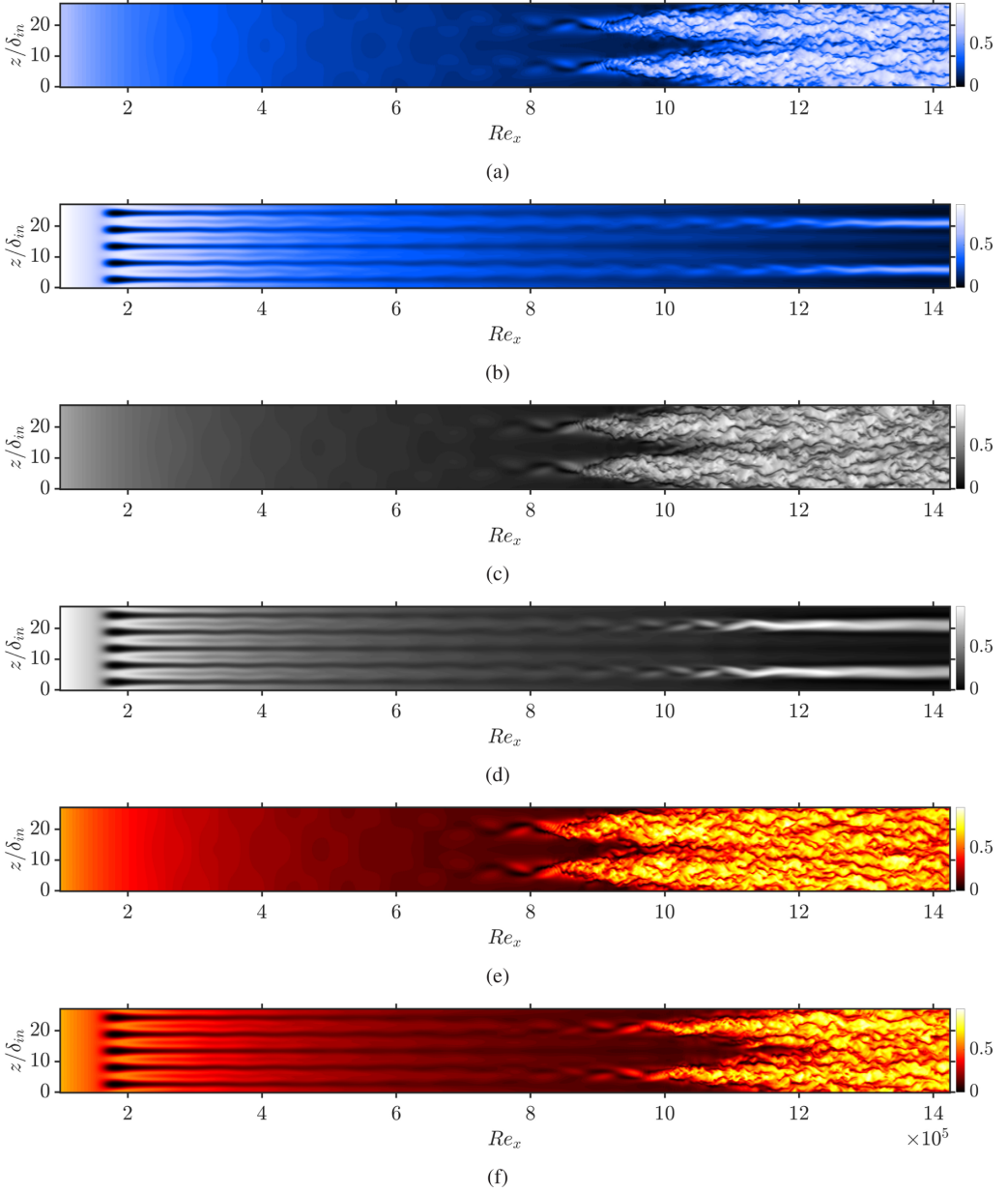


FIG. 4. Contours of u/u_∞ at $y/\delta_{in} = 0.517$ in an instantaneous flow-field for (a) C_T , (b) $C5C$, (c) A_T , (d) $A5C$, (e) H_T , and (f) $H5C$ scenarios.

Simulations are carried out for slightly heated, $T_w = 1.05 \times T_{aw}$, and slightly cooled, $T_w = 0.95 \times T_{aw}$ wall conditions. Results are compared with those of adiabatic wall cases.

Figure 4 illustrates the nondimensional streamwise velocity contour taken inside the boundary layer at $y/\delta_{in} = 0.517$ in the x - z plane for cases with and without control streaks. Note that the transition-to-turbulence takes place in all the control-free scenarios. Therefore, a comparison between control-free cases shows, although not explicitly in Fig. 4, stabilizing/destabilizing effect of cooling/heating, as predicted by LST, see the discussion of Fig. 5 below. Similar behavior in

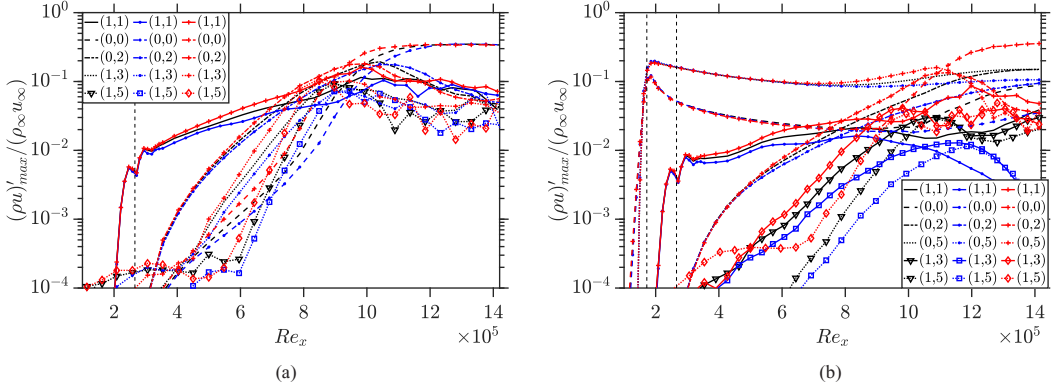


FIG. 5. Streamwise evolution of the maximum disturbance amplitudes of various disturbance modes for the cases (a) without C_T , A_T , and H_T and (b) with control streaks $C5C$, $A5C$, and $H5C$. Cooled (\bullet , \square), adiabatic ($-$, $-\nabla$), and heated ($+$, \diamond) scenarios.

flow stabilization by cooling is also reported by Kneer [23]. Concerning the cases with control streaks, the formation of streamwisely elongated steady vortices is represented by the superposition of streaky modes $(0,2)$, $(0,4)$, $(0,6)$, observed in $A5C$ and $C5C$ in the downstream direction. They regulate the flow field by transporting high-momentum fluid from the external boundary layer to the near wall regime. Thereafter, the flow stays laminar in $A5C$ and $C5C$ scenarios, whereas the streaks break down to turbulence as they are strongly amplified in $H5C$.

For a better understanding of the propagation of disturbances and their possible breakdown mechanism, the streamwise evolution of various disturbance modes is plotted in Fig. 5. Concerning the control-free scenarios, exponential growth of the fundamental disturbance $(1,1)$ is followed by fully nonlinear behavior indicating a flow transition farther downstream in all the cases. The earliest in the heated (H_T) and the latest in the cooled (C_T) are marked, as shown in Fig. 5(a). For a given streamwise location, it is seen that both the maximum disturbance amplitude and the growth rate of any mode are the highest for H_T and the lowest for C_T once the modes reach significant amplitudes. After having generated, the steady mode $(0,2)$ drives the flow to transition with the contribution of $(1,1)$ and nonlinearly generated modes, i.e., $(1,3)$, $(1,5)$, and so on. Close to the end of the computational domain, the MFD $(0,0)$ attains the highest amplitude, indicating a strong mean flow deformation due to transition to turbulence. When the control strip is activated, see Fig. 5(b), the presence of the control mode $(0,5)$ leads to an earlier generation of the MFD in all cases, as mentioned in Sec. III A. It is seen that the MFD carries approximately the same value until around a point where the steady mode $(0,2)$ gains significant amplitude. Then $H5C$ deviates from the cases at around $Re_x = 9 \times 10^5$. Here the steady mode $(0,2)$ will be used for marking the presence of transition in the domain since sudden changes in MFD could also be an indication of sharp but regular deformation of the flow field. In doing so, it could be deduced that the laminar flow regime is preserved until the end of the computational domain in $A5C$ and $C5C$, whereas the transition in $H5C$ is postponed to downstream without being able to completely avoid it. Moreover, the fundamental mode $(1,1)$ for the cooled scenario ($C5C$) is fully attenuated after having reached its maximum value at around $Re_x = 8 \times 10^5$. This is a definite sign of flow staying laminar.

There exist various parameters which have been exploited to pinpoint the flow transition and its onset location in the literature. Among others, the skin-friction coefficient is illustrated as a function of streamwise direction in Fig. 6. Stabilizing effect of wall cooling, as predicted by LST [30] and experimentally for a wide range of Mach numbers [31], is evidently seen for control-free scenarios in Fig. 6(a). Having traced the laminar skin-friction coefficient trend, transition onset is observed the earliest in H_T and the latest in C_T . When the flow breaks down to turbulence, the order is inverted in terms of the magnitude of the turbulent skin-friction coefficient. The reason is

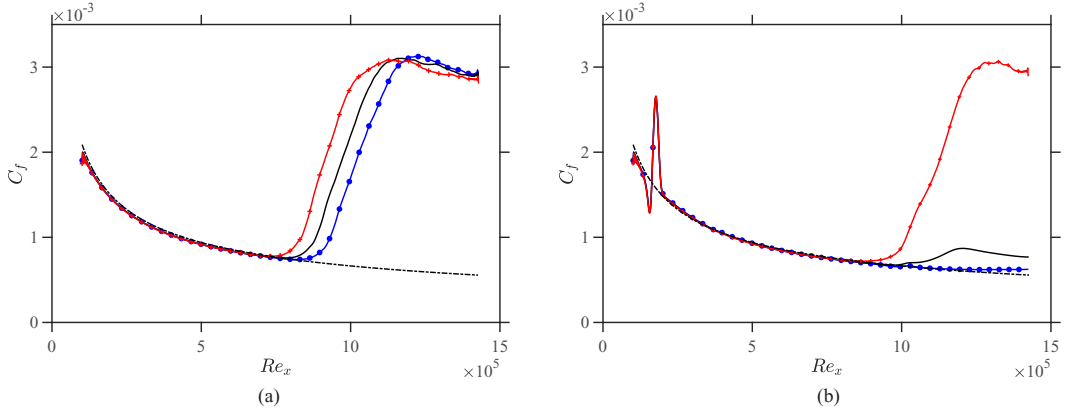


FIG. 6. Streamwise evolution of skin-friction coefficient for (a) control-free cases (C_T , A_T , and H_T) and (b) controlled cases ($C5C$, $A5C$, and $H5C$) where cooled (\bullet), adiabatic ($-$), and heated ($+$). Skin-friction coefficient for laminar flow ($--$) estimated by [29] $C_f = 0.664/\sqrt{Re_x}$.

attributed to the higher velocity gradient of the cooled scenarios in the wall-normal direction. Since the dynamic viscosity scales up with temperature which is inversely proportional to the density, wall cooling results in a lower air kinematic viscosity, so does a thinner boundary layer compared to the heated cases. Although the dynamic viscosity is lowered with the temperature decrease, higher velocity gradient due to lower boundary-layer thickness is dominant and causes a higher skin-friction coefficient. Concerning the cases with control streaks, Fig. 6(b) illustrates their skin-friction coefficient evolution in the streamwise direction. The kinks corresponding to the location of the control strip are generated due to control streaks. All the profiles follow the laminar skin-friction trend, to a streamwise location corresponding to about $Re_x = 8 \times 10^5$ from which a prominent deviation can be observed in $H5C$. This deviation corresponds to a region between $Re_x = 8.5 \times 10^5$ and $Re_x = 10^6$ in Fig. 4(f), where a formation of two high-velocity streaks becomes visible in addition to the control streaks. Since they rapidly break down to turbulence further downstream, their formation in $H5C$ is relatively discrete compared to the adiabatic counterpart ($A5C$), see Fig. 4(d). The concerning breakdown mechanism exhibits its impact on the skin-friction coefficient with a drastic augmentation around $Re_x = 10^6$ for $H5C$. Contrarily, these nonlinearly generated streamwise vortices last longer in the streamwise direction and reach the end of the computation domain for $C5C$ and $A5C$. The boundary layer gets thinner in the proximity of these streaks which results in a steeper velocity gradient at the wall in the case of $A5C$. Consequently, the skin-friction coefficient makes a slight augmentation around $Re_x = 10^6$, followed by a decrease with a slope similar to that in the laminar regime while the flow remains laminar until the end.

In addition to the maximum amplitude of various disturbances, the shape of a disturbance with respect to the wall-normal direction should also be looked at to understand its evolution inside the boundary layer. Prior to the isothermal boundary condition, the nonlinear transitional regime is elaborated for the adiabatic wall condition. The most significant modes in oblique breakdown are plotted and a comparison between A_T and $A5C$ scenarios is provided in Fig. 7. Figure 7(a) depicts the evolution of the MFD in the presence and absence of the control mode. Herein, an early generation of the MFD can be seen with the control streaks. Although its maximum amplitude already decreased from 12% to 3% of $\rho_\infty u_\infty$ from its generation to the first streamwise location, its maximum amplitude is still substantially higher than that of A_T until $Re_x = 8 \times 10^5$. For A_T , the MFD attains a positive amplitude near the wall making the mean flow profile fuller as the onset of transition is reached at $Re_x = 8 \times 10^5$. However, the MFD in $A5C$ stabilizes the flow since its generation, by impressing a fuller velocity profile in the boundary layer with positive values in the inner boundary layer and negative values in the outer two-thirds of the boundary layer. It is seen

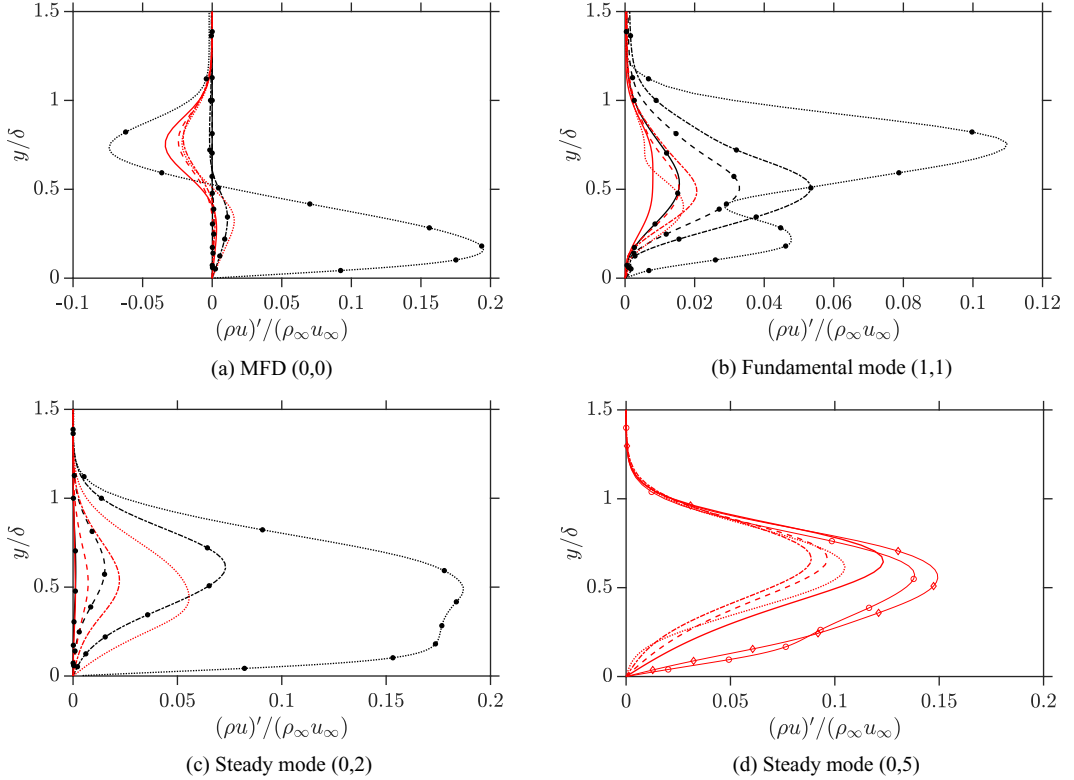


FIG. 7. Disturbance amplitude of various modes for A_T (\bullet) and $A5C$ ($-$) obtained at $Re_x = 4 \times 10^5$ ($-$), $Re_x = 6 \times 10^5$ ($--$), $Re_x = 8 \times 10^5$ ($- \cdot -$) and $Re_x = 10 \times 10^5$ (\cdots) with respect to the wall-normal direction. Two additional locations are given (d) at $Re_x = 12 \times 10^5$ ($-o$) and $Re_x = 14 \times 10^5$ ($- \diamond$). δ denotes the local boundary-layer thickness.

that the distortion of the control streaks (0,5) manifests itself relatively higher in the upper half of the boundary layer. Going downstream the maximum MFD amplitude, the MFD is overtaken by the steady mode (0,2) at around $Re_x = 8 \times 10^5$ in $A5C$. Once the steady modes (0,2), (0,4), (0,6), etc., turn into streamwise elongated vortices, the positive shape of the profile is expanded in the boundary layer, making the profile antisymmetric centered at about half of the boundary-layer thickness. Following a linear modulation, the fundamental mode (1,1) for A_T consistently grows while carrying its maximum at around $y/\delta = 0.5$ until $Re_x = 8 \times 10^5$, see Fig. 7(b). There, the flow experiences a flow transition that strongly modifies the shape of the disturbance profile generating a second hump in the inner half of the boundary layer. With the presence of the control streaks (0,5) in $AC5$, the amplitude increase of the fundamental mode in each fluid layer is attenuated. Regression, also observed in Fig. 5(b) for the maximum disturbance amplitude, is observed in the upper two-thirds of the boundary layer at $Re_x = 10^6$. Although not shown here, for concision, the regression is compensated once the fundamental mode starts growing after $Re_x = 1.1 \times 10^6$. However, its maximum amplitude never goes beyond 2.3% of $\rho_\infty u_\infty$ in $A5C$. The strong damping of the fundamental mode reflected itself in the growth rate and the amplitude profile of the steady mode (0,2) as shown in Fig. 7(c). Although its growth rate is reduced with the presence of the control streaks, it still persistently increases in amplitude until the end of the computational domain in $A5C$. Contrary to the shift of the profile closer to the boundary-layer edge in A_T , the profile approaches the wall with an increased maximum disturbance amplitude in $AC5$. Having obtained significant amplitudes at $Re_x = 10^6$, it leads to the generation of two high-velocity streaks with the contribution

of its integer multiples, i.e., (0,4), (0,6), and so on, see Fig. 4(b). On the other hand, the profile of A_T is distinctively distorted at $Re_x = 10^6$ with the fully nonlinear effects followed by a flow transition further downstream. Besides, the control mode (0,5) is represented with two additional streamwise positions in Fig. 7(d). Following its evolution, the amplitude of the control mode in each fluid layer decreases until $Re_x = 6 \times 10^5$. Moving downstream, the control mode starts to grow and its profile gets distorted in the inner half of the boundary layer after $Re_x = 8 \times 10^5$ as a consequence of high-amplitude steady modes.

Regarding the influence of the isothermal wall condition on the disturbances, Fig. 8 depicts the shape evolution of various modes in the boundary layer obtained at four different streamwise locations for cooled, adiabatic, and heated boundary conditions. The extraction is done at points where the deviations between the cases become significant. Nonlinear PSE calculations of Chang and Malik [7] asserted that negative values of the MFD indicate an energy transfer extracted from the mean flow and transferred to the unsteady disturbances. It is seen that the MFD retains only positive values near the wall in all cases, yielding a fuller velocity profile as the flow goes toward transition to turbulence, denoting the energy transfer from the disturbances to mean flow, see Fig. 8(a). Also, it is observed that H_T is the first scenario bearing relatively high negative values at $Re_x = 9 \times 10^5$ in the upper boundary layer compared to the cooled and adiabatic cases. This corresponds to the position at which the MFD starts taking over the fundamental disturbance (1,1), where the flow enters the late nonlinear regime [11], see Fig. 5(a). The MFD maximum gets closer to the wall with the positive region shrinking and approaching the wall. Meanwhile, the region of negative values occupies two-thirds of the boundary layer corresponding to its outer part. This identical trend is observed in each scenario. With transition to turbulence, the MFD attains the maximum disturbance amplitude representing the shape change of the mean-velocity profile from its laminar to the turbulent shape, induced by the action of the Reynolds stresses. The evolution of the fundamental mode (1,1) shows that its peak amplitude appears closer to the boundary-layer edge as the wall is heated, whereas it gets closer to the wall if it is cooled down, as shown in Fig. 8(c). As soon as the onset of transition is reached, the profiles are distorted due to strong nonlinear effects. As for the steady mode (0,2), based on the terminology of Mayer *et al.* [11], the point corresponding roughly to a position where (0,2) and (1,3) reach the same order of amplitude indicates the end of the early transition regime. Being the characteristic for the oblique breakdown mechanism, distortion in its wall-normal profile can be interpreted as the inception of strong nonlinear interactions in the flow domain. Besides, the cooling diminishes the growth of the mode causing it to have a lower maximum amplitude, whereas its influence is reversed in the inner boundary layer at $Re_x = 7 \times 10^5$, see Fig. 8(e). Further downstream, the shape of the profiles gets more bumper in the lower half of the boundary layer, earliest in the heated case, latest in the cooled scenario, indicating strong nonlinearities.

It was pointed out previously that the presence of streaks leads to an earlier generation of the (0,0) mode. Although it reaches 12% of $\rho_\infty u_\infty$ at the control strip location, it decreases up to 3% of $\rho_\infty u_\infty$ at $Re_x = 7 \times 10^5$, see Fig. 8(b). As indicated in Fig. 8(a), the region with positive values moves closer to the wall as the boundary layer grows, whereas the negative zone expands in the boundary layer. Also, significant increase is seen in $H5C$ at $Re_x = 11 \times 10^5$ and $Re_x = 13 \times 10^5$ that indicates the flow transition. The combined stabilizing effect of cooling and induced control modes is clearly seen in the damping of (1,1) as the flow proceeds downstream, see Fig. 8(d). It is not only the maximum value of the disturbance amplitude but also the entire profile which experiences the regression. However, flow transition is observed in $H5C$ with a maximum amplitude growing in the streamwise direction. Its profile is fully distorted with a second peak much closer to the wall holding a value more than half of its maximum at $Re_x = 13 \times 10^5$. On the other hand, $A5C$ experiences an exponential amplification in the fundamental mode until its saturation at around $Re_x = 7 \times 10^5$. Having reached the saturation with around 2% of $\rho_\infty u_\infty$, the maximum amplitude retains its value until $Re_x = 10^6$ after which it experiences an exponential increase until the end of the domain. As long as the flow remains laminar, the maximum disturbance amplitude of the steady vortex mode (0,2) gets closer to the wall as the flow develops, regardless of the wall boundary condition, see Fig. 8(f). Its active role in regulating the flow field gets stronger as it gets closer to

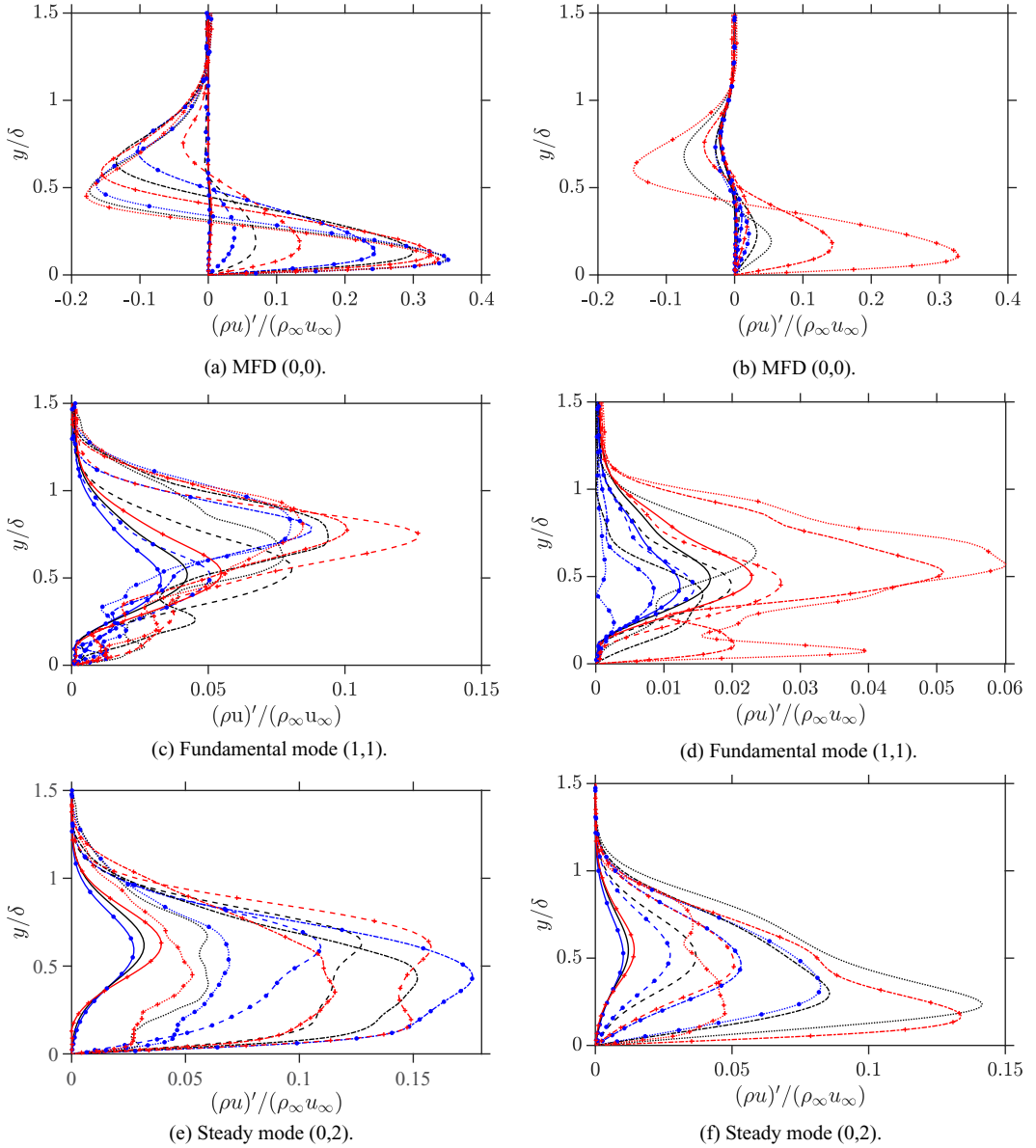


FIG. 8. Disturbance amplitude of trademark modes in oblique breakdown as a function of the wall-normal direction at $Re_x = 7 \times 10^5$ (—), $Re_x = 9 \times 10^5$ (---), $Re_x = 11 \times 10^5$ (-·-·), $Re_x = 13 \times 10^5$ (····). Cooled (●), adiabatic (—), and heated (+) scenarios. The left column indicates the control-free cases (C_T , A_T and H_T), whereas $C5C$, $A5C$ and $H5C$ are illustrated on the right side.

the wall with a maximum disturbance amplitude reaching up to 14% of $\rho_\infty u_\infty$ and 8% of $\rho_\infty u_\infty$ for $AC5$ and $C5C$, respectively. Further downstream, a hump starts to form in the outer half of the boundary layer in all scenarios. The disturbance profile of $H5C$ becomes significantly distorted once the flow becomes turbulent. Experiencing a saturation, $A5C$ preserves its maximum amplitude for a longer streamwise distance in (0,2), see Fig. 5(b), while its profile attains the highest amplitude in the entire boundary layer compared with $C5C$ and $H5C$. Besides, the wall cooling reduces the

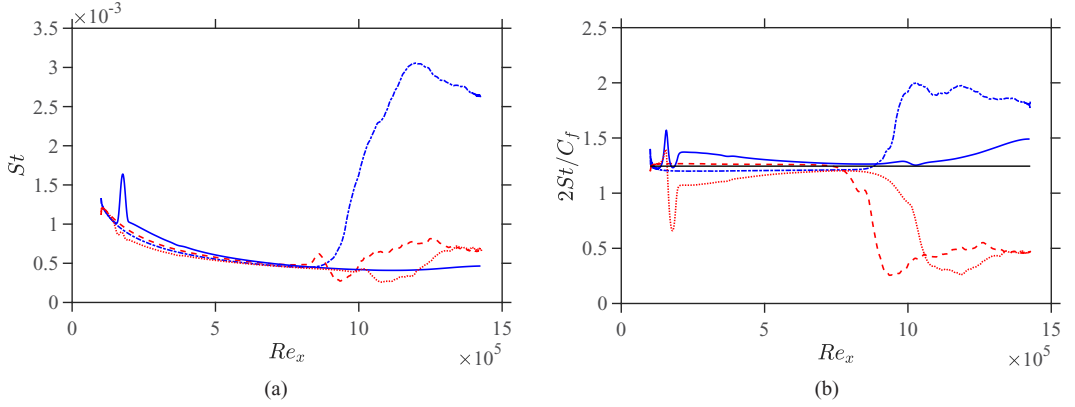


FIG. 9. Streamwise evolution of (a) Stanton number (St) and (b) Reynolds analogy factor ($2St/C_f$), whereas horizontal solid line on the right figure is $Pr^{-2/3}$. C5C (—), C_T (---), H5C (---), and H_T (.....).

amplitude growth of the steady mode and keeps its maximum always at a higher location in the wall-normal direction compared to A5C and H5C before transition occurs in the heating scenario.

As a dimensionless parameter, the Stanton number is a measure of the wall heat-transfer rate and is defined as $St = q_w / [\rho_\infty U_\infty C_p (T_{aw} - T_w)]$ where q_w is the heat transfer rate from the wall and is calculated as $q_w = -k(\partial \langle \bar{T} \rangle_z / \partial y)|_{y=0}$. Here the overbar and “ $\langle \rangle$ ” denote time- and space averaged quantities, respectively. Being the adiabatic wall temperature for a laminar boundary layer, T_{aw} is estimated with $T_{aw} = T_\infty [1 + r(\gamma - 1)/2 \times M_\infty^2]$ where r is the recovery factor. For laminar flow [29], $r = \sqrt{Pr}$. As the definition of Stanton number is based on adiabatic wall temperature for laminar flows, its values for turbulent and transitional regimes should solely be treated qualitatively. Figure 9(a) shows the streamwise evolution of the Stanton number for isothermal scenarios. Heat transfer is found to be strongly influenced by the control streaks which alter the Stanton number in favor of the C5C as opposed to the control-free cases. However, they all converge until the earliest transition onset which is observed in H_T. From this point onward, a significant variation between the scenarios reveals itself. It is observed that the rate of heat transfer becomes 5 to 6 times higher for C_T than C5C as a result of a marginally steeper temperature gradient near the wall in the absence of the control mechanism as shown in Fig. 10. As for H5C, following a delayed transition in the presence

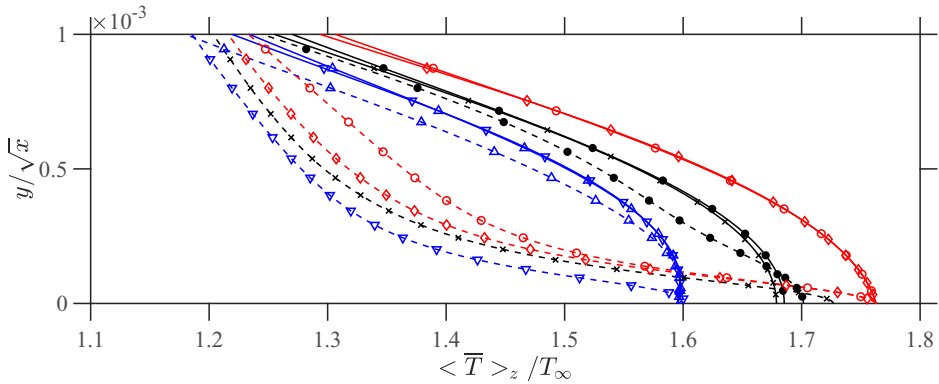


FIG. 10. Temperature profiles at $Re_x = 4.3 \times 10^5$ (solid lines) and $Re_x = 12.57 \times 10^5$ (dashed lines). C_T (Δ), C5C (∇), A_T (\times), A5C (\bullet), H_T (\circ), and H5C (\diamond).

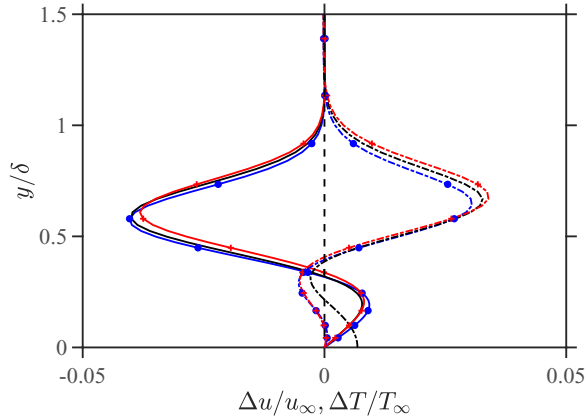


FIG. 11. Mean temperature $\Delta T = \langle \bar{T} \rangle_z - T_b$ profile (dashed lines) and mean streamwise velocity component (solid lines) $\Delta u = \langle \bar{u} \rangle_z - u_b$ at $\text{Re}_x = 3 \times 10^5$ for C5C (●), A5C (—), and H5C (+).

of the control streaks, an initial reduction ensued by an increase toward downstream where St meets its control-free counterpart of H_T toward the end of the domain. Furthermore, direct relation between the shear stress and the heat transfer is provided by the Reynolds analogy factor $2\text{St}/C_f = \text{Pr}^{-2/3}$, which serves as a useful tool in practical applications to estimate the heat transfer rate through the skin-friction coefficient [32]. They all converge, rather slower in the control-free cases, to the $\text{Pr}^{-2/3}$, see Fig. 9(b). In the sequel of the transition onset, the cases drift apart with a decrease in the heated scenarios and a rise in C_T . Moving further downstream, the increase both in the Stanton number and the skin-friction coefficient due to the formation of two-high velocity streaks increase the Reynolds analogy factor in C5C.

In an attempt to consider the influence of the boundary-layer growth in the streamwise direction, knowing that the boundary-layer thickness is proportional [33] to \sqrt{x} , Fig. 10 is plotted with respect to y/\sqrt{x} . It is seen that employing the velocity streaks decreases the temperature gradient at the wall and retains the laminar temperature profile for C5C at $\text{Re}_x = 12.57 \times 10^5$. When no control is applied, the cooled wall scenario (C_T) attains a turbulent profile with identical wall temperature as the rest of the cooled scenarios but with a steeper temperature gradient. This gradient is the main reason for observing a tremendous increase in the Stanton number in Fig. 9(a). As for the heated cases (H5C, H_T), it is seen that the presence of the control streaks does not carry any significance at the wall, but they modify the temperature profile at the first streamwise location. Given that $\text{Re}_x = 12.57 \times 10^5$ corresponding to the turbulent regime in both H_T and H5C, they present steeper temperature profiles. Adiabatic cases, on the other hand, show different trends compared to the isothermal scenarios. The presence of velocity streaks generates a marginally higher wall temperature at the wall at $\text{Re}_x = 4.3 \times 10^5$, which increases downstream following the formation of high-velocity streaks with a modified temperature profile. Once the control mechanism is discarded, the flow becomes turbulent with a wall temperature equal to the adiabatic wall temperature of turbulent flow at the second streamwise location, $\text{Re}_x = 12.57 \times 10^5$. Kneer [23] reported similar behaviors for adiabatic and cooled wall scenarios.

Figure 11 represents the mean flow temperature and velocity profiles in order to scrutinize the stabilizing influence of the MFD (0,0) stated by Paredes *et al.* [20]. It is seen that the flow is accelerated near the wall with the induction of the streaks, whereas it decelerates in the outer region of the boundary layer. Thus, a fuller velocity profile is provided indicating a more stable flow [34]. Contrarily, the temperature field exhibits an opposite behavior such that the flow is slightly cooled down in the inner boundary layer, whereas it is heated in the outer part. However, there exists a region where the fluid is heated in the adiabatic scenario close to the wall as illustrated in Fig. 10 with respect to A_T . While the role of heating/cooling continuously changes in the wall-normal

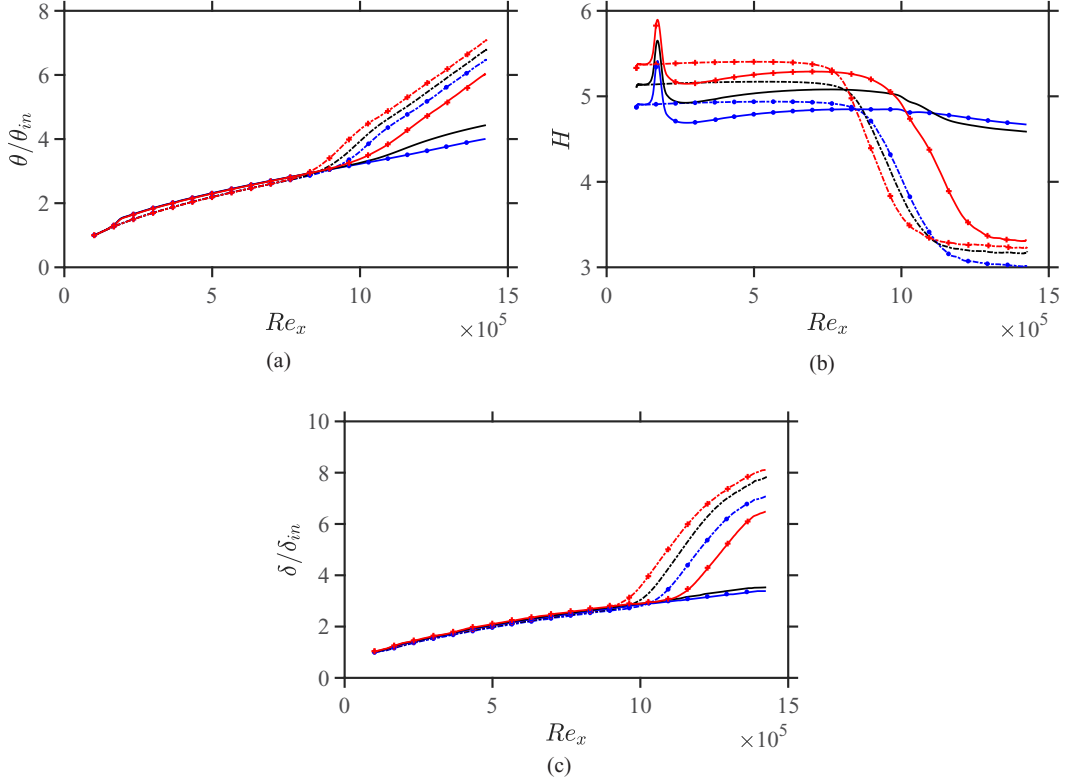


FIG. 12. Streamwise evolution of (a) momentum thickness, (b) shape factor, and (c) boundary-layer thickness. Control-free cases (dashed lines), control cases (solid lines) wherein cooled (\bullet), adiabatic ($-$), and heated ($+$).

direction in terms of the velocity profile, it is decidedly seen that H5C has the highest heating and the lowest decelerating impact on the fluid in the outer boundary layer.

The streamwise evolution of the momentum thickness is presented in Fig. 12(a). The profiles in each case follow a smooth trend in the laminar region except for the location where the earlier appearance of the MFD becomes evident due to the control streaks. It is seen that the growth rate increases drastically once the flow becomes turbulent in control-free and H5C cases. Besides, the highest value is obtained always for the case with earliest transition. Cooling has been one of the common techniques to achieve a fuller velocity profile for air-flow stabilization [35] which consequently decreases the shape factor. The presence of the control mode (0,5) results in an instantaneous decrease in the shape factor at the beginning of the domain as shown in Fig. 12(b). In that way, transition is avoided in A5C and C5C, whereas the shape factor of H5C decreases further downstream with regard to H_T that indicates a delay in the heated scenarios. Despite having a fuller velocity profile in the boundary layer, the presence of the streaks resulted in thickening the boundary layer, see Fig. 12(c). Although there exists a minute difference in control cases due to the low rate of heating/cooling at the wall, an increase in kinematic viscosity due to temperature increase has a significant impact on the boundary-layer development.

Figure 13 shows the streamwise vorticity contours obtained at various downstream positions for A_T and $A5C$. Structural flow development is analyzed only for the adiabatic scenario after having concluded that weak heating/cooling does not exhibit a significant impact on the general flow structures. Concerning the control-free case, the evolution of the disturbances is accompanied by the opposite signs of vorticity values due to their obliquely running nature, are depicted in Fig. 13(a) at

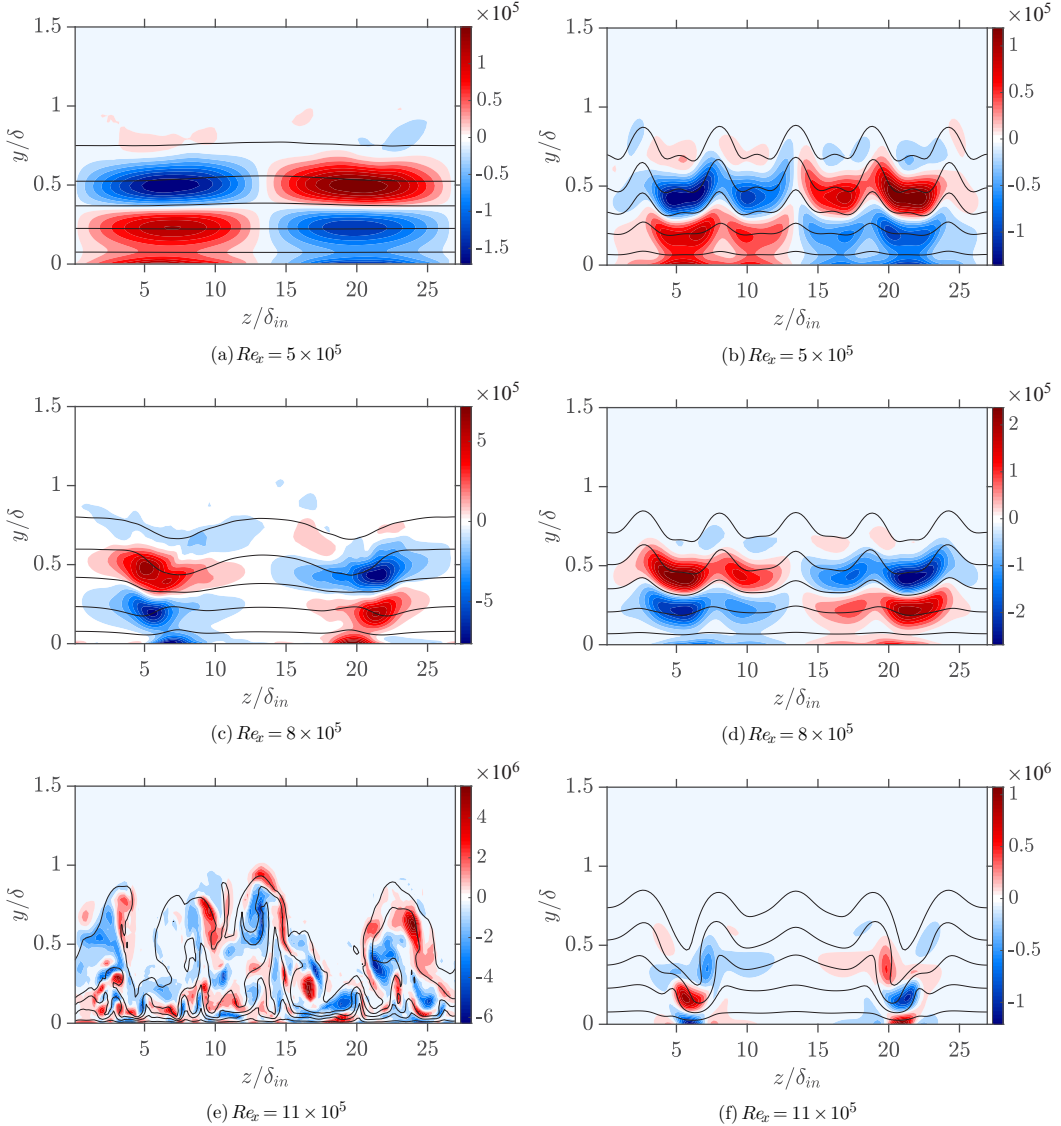


FIG. 13. Streamwise vorticity (ω_x) contours of an instantaneous flow-field at various streamwise positions for A_T (left row) and ASC (right row). The black solid lines are isolines of streamwise velocity component with $0.1, 0.3, 0.5, 0.7,$ and $0.9 \times u_\infty$.

$Re_x = 5 \times 10^5$. Further downstream, the steady mode (0,2) having maximum disturbance amplitude of 8% of $\rho_\infty u_\infty$, see Fig. 5(a), shows its impact on the flow by prominently distorting the streamwise vorticity field in Fig. 13(c). At around $Re_x = 9 \times 10^5$, the onset of the transition appears in the domain, leading the flow to transition where a fully nonlinear regime prevails in the field resulting the formation of small near-wall structures as illustrated in Fig. 13(e). Once the control streaks are applied, the strong flow field regulation, visualized in the x - z plane in Fig. 4(d), can also be seen for the vorticity field in Fig. 13(b) with some deformation in the inner boundary. Following the growth of the disturbance modes, deformation is reflected in the vorticity field at $Re_x = 8 \times 10^5$ as seen in Fig. 13(d). Further downstream, high deformation due to strengthened steady modes is observed

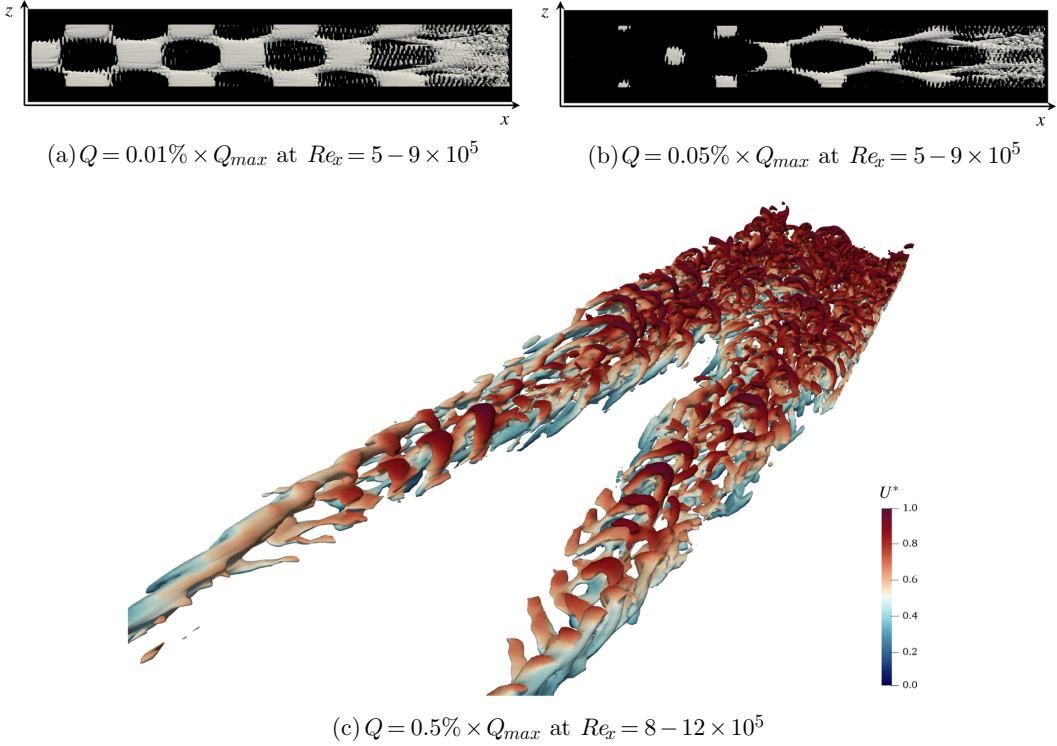


FIG. 14. Isosurfaces of Q criterion for A_T : [(a) and (b)] Top view and (c) 3D view. $U^* = (u - u_{min}) / (u_{max} - u_{min})$.

with its clear physical domination of the flow field in Fig. 13(f). The fluid retains its regular structure with the formation of two high-velocity streaks, while the boundary-layer properties remain akin to those of the laminar flow until the end of the computational domain.

The vortical structures developed in A_T are identified by the Q criterion [36] in Fig. 14 (Q being the second invariant of the velocity gradient, which defines the vortical regions where the vorticity magnitude is larger than that of the strain rate). Figure 14(a) illustrates the superposition of the fundamental oblique wave traveling in the opposite spanwise directions. The formation of honeycomb-like structure is seen as reported by Bestek *et al.* [8]. Moving downstream, its shape is distorted due to the steady modes that are rapidly growing. When the Q criterion is increased, the vortical structures generated due to steady modes become visible, see Fig. 14(b). To accurately display the transitional and the turbulent regimes, a 3D flow-field visualization is used in Fig. 14(c). Proceeding to the onset of transition at around $Re_x = 8 \times 10^5$, the formation of ring-shaped vortices are marked in the figure. Further downstream, the identification of hairpin vortices is a clear evidence of a fully turbulent boundary layer in the domain. A similar study is carried out for $A5C$ to reveal the influence of the control streaks in the flow development. The presence of the control streaks regulates the flow field by damping the disturbances in Figs. 15(a)–15(b). Besides, an increase in Q criterion highlights the formation of the steady modes in the domain. With the 3D view of the flow field, it is observed that no transitional regime is reached by the end of the domain, see Fig. 15(c). Therefore, a successful transition delay is proven to be sustained once again in the presence of the control mode (0,5).

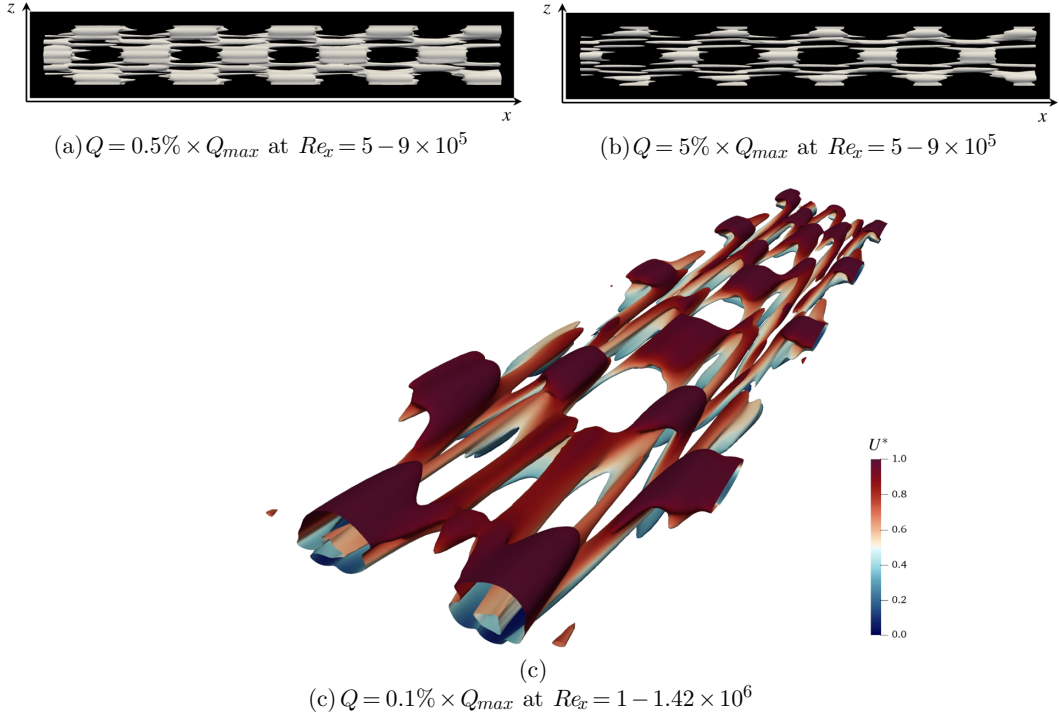


FIG. 15. Isosurfaces of Q criterion for A5C: [(a) and (b)] Top view and (c) 3D view. $U^* = (u - u_{min}) / (u_{max} - u_{min})$.

C. Parametric study

Preceding the effective transition delay of the current strategy, the question as to what extent this method could be applied should be answered. In that way, an extensive parametric study is carried out for adiabatic and weakly cooled/heated walls for a wide range of the control strip amplitudes. Velocity contours obtained at $y/\delta_{in} = 0.517$ are illustrated in Figs. 16–18 representing cooled, adiabatic and heated scenarios, respectively. Here, the applied control amplitude is in the range of $A_{c,ref} \times 0.25 \leq A_c \leq A_{c,ref} \times 2.0$ where $A_{c,ref} = 1.22 \times 10^{-2}$, identical to the control amplitude in Sec. III A. Also, an effective transition control is defined for those where transition is delayed until the end of the computational domain. What could be generally seen in these figures is that below a certain threshold of the control amplitude, the transition scenario is akin to the control-free cases. Similar behavior is observed by Sharma *et al.* [21] and Kneer [23] when the control amplitude is halved although their control amplitude was reported to be differing by a factor of 2 among each other. Furthermore, a drastic change in flow is observed with a successful transition delay when the amplitude is increased above certain value, i.e., $A_c \geq 0.7 \times A_{c,ref}$ for cooled, $A_c \geq 0.9 \times A_{c,ref}$ for adiabatic and $A_c \geq 1.2 \times A_{c,ref}$ for the heated cases. However, contrary behavior in the flow field is seen for the upper threshold amplitude. When the amplitude is increased from 1.7 to 1.8 $\times A_{c,ref}$, an earlier transition onset compared to the control-free scenarios is observed no matter the thermal boundary condition. The study of streamwise evolution of various disturbance modes revealed that the MFD (0,0), the control mode (0,5), and the integer multiples of the control mode are the only increasing modes among all. Therefore, the immediate shift in transition onset is concluded to be due to streak instabilities which induce bypass transition according to Parades *et al.* [37,38]. They also reported an approximate saturation of the transition onset location following a sufficiently high amplitude reached by the streaks. This is reflected in the present study once the amplitude goes

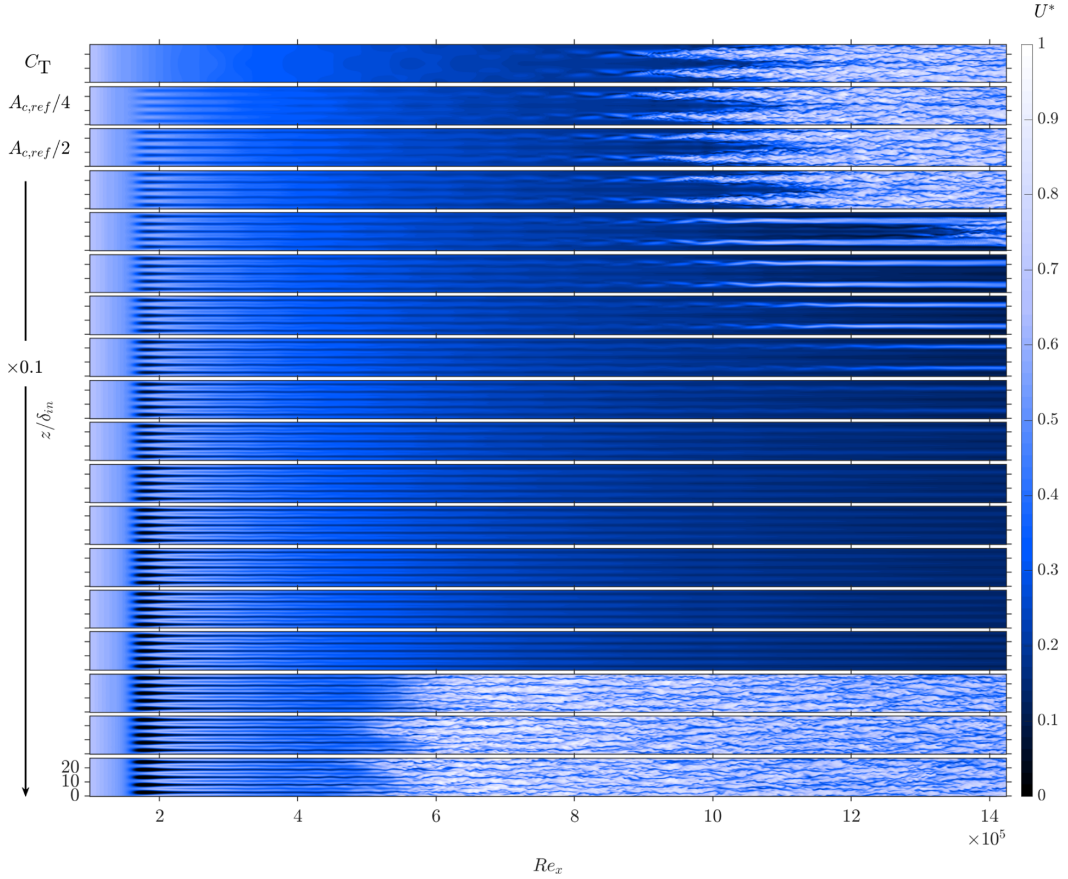


FIG. 16. Contours of $U^* = (u - u_{\min}) / (u_{\max} - u_{\min})$ at $y/\delta_{\text{in}} = 0.517$ in an instantaneous flow-field for various control amplitudes in the cooled scenarios. From top to bottom, the first one designates C_T , whereas the trailing two ones are the control cases with $A_c = 0.25 \times A_{c,\text{ref}}$ and $A_c = 0.5 \times A_{c,\text{ref}}$, respectively. Then, the increase of control amplitude is by 0.1 in the direction of the arrow.

1.7 times higher than the reference control amplitude. However, additional simulations indicate that transition might even be induced immediately after the control strip in case of higher control amplitudes than the maximum value used here. All in all, cooling increases the range of amplitude for which a successful transition could be sustained whereas heating inversely impacts by reducing the range of application. Besides, heating is found to be carrying higher influence on the flow in terms of control amplitude range modification compared to cooling. As shown in the present study, Sharma *et al.* [21] reported an earlier flow transition when the amplitude is doubled for an oblique breakdown initiated solely by a pair of three-dimensional disturbances. However, more effective dampening is pointed out by Kneer [23] in the presence of subharmonic disturbances in addition to that of the fundamental one. Therefore, the control amplitude range of the streak-employing strategy is found highly case dependent. Additionally, the effectiveness of the control streak mode (0,4) should be investigated since it was also found beneficial in delaying transition for the identical flow/geometry configuration with adiabatic wall [21]. Therefore, although the results are not presented here, a parametric study with (0,4) has also been carried out for the same range of control amplitudes. The study has been performed only for the adiabatic wall condition and the effective range is found to be in the range of $A_{c,\text{ref}} \times 0.7 \leq A_c \leq A_{c,\text{ref}} \times 1.2$. It is seen that the low-level threshold of (0,4) is lower than that of (0,5) whereas a significant difference is observed in terms of

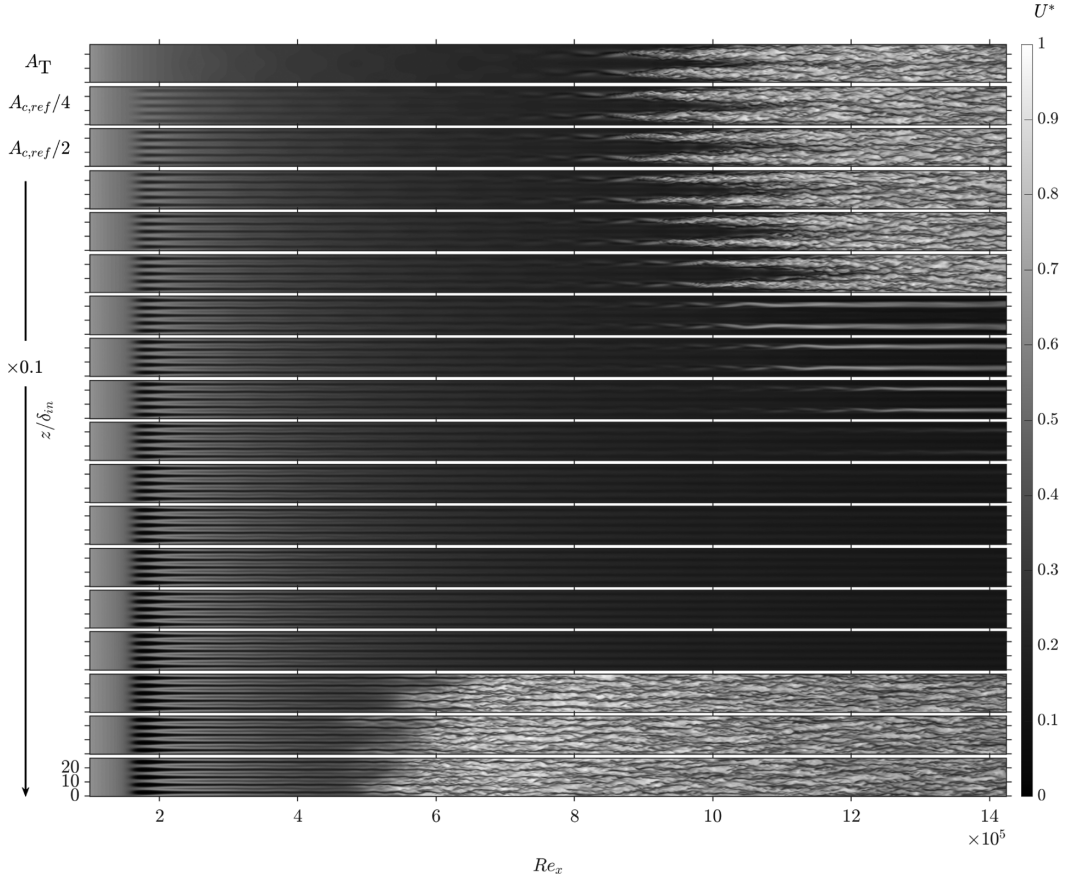


FIG. 17. Contours of $U^* = (u - u_{\min}) / (u_{\max} - u_{\min})$ at $y/\delta_{in} = 0.517$ in an instantaneous flow-field for various control amplitudes in the adiabatic scenarios. From top-to-bottom, the first one designates A_T , whereas the trailing two ones are the control cases with $A_c = 0.25 \times A_{c,ref}$ and $A_c = 0.5 \times A_{c,ref}$, respectively. Then the increase of control amplitude is by 0.1 in the direction of the arrow.

their applicable range for successful transition control. A comparison in terms of $(\rho u)'_{\max} / (\rho_{\infty} u_{\infty})$ shows, 16.8–24.1% for (0,4) and 18–25.8% for (0,5), estimated at the control strip. The summary of the effective range of control amplitudes for the studied scenarios are summarized in Table II.

TABLE II. The range of the control streaks amplitude for effective transition control.

Cases	T_w/T_{aw}	Control mode	$A_c/A_{c,ref}$ (%)	$(\rho u)'_{\max} / (\rho_{\infty} u_{\infty})$ (%)
A5C	1	(0,5)	90–170	18–25.8
A4C	1	(0,4)	70–120	16.8–24.1
C5C	0.95	(0,5)	70–170	15.8–26.5
H5C	1.05	(0,5)	120–170	20.8–25.2

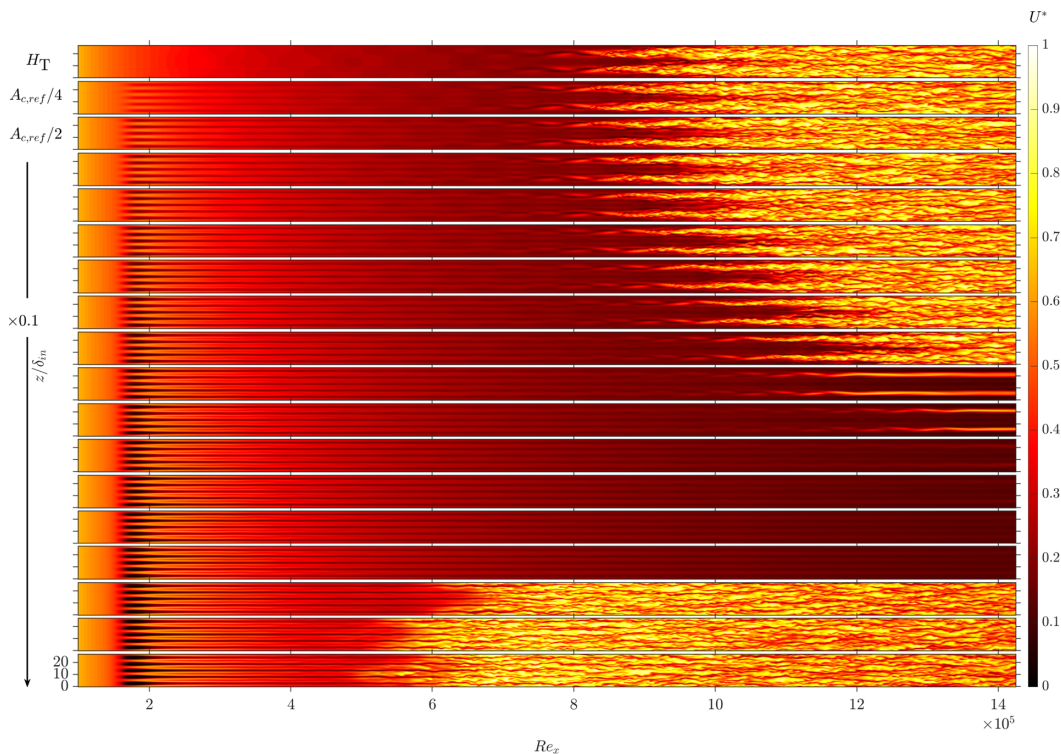


FIG. 18. Contours of $U^* = (u - u_{\min}) / (u_{\max} - u_{\min})$ at $y/\delta_{\text{in}} = 0.517$ in an instantaneous flow-field for various control amplitudes in the heated scenarios. From top to bottom, the first one designates H_T , whereas the trailing two ones are the control cases with $A_c = 0.25 \times A_{c,\text{ref}}$ and $A_c = 0.5 \times A_{c,\text{ref}}$, respectively. Then, the increase of control amplitude is by 0.1 in the direction of the arrow.

IV. CONCLUSIONS

In an attempt to investigate the effectiveness of the use of velocity streaks in delaying boundary-layer transition under the influence of wall heat transfer, perturbed supersonic flows at $M_\infty = 2$ were investigated by means of direct numerical simulations. The most-amplified disturbance, estimated for the adiabatic wall condition, was retained for the isothermal walls. In doing so, the isolated impact of weak heating/cooling could be evaluated rigorously. The control streaks are introduced using an additional blowing/suction strip placed right in front of the perturbation strip. The steady streaks (0,5), which was reported to be the most effective mode in delaying transition, were assessed for a wide range of control amplitudes. Initially, a stabilizing/destabilizing influence of cooling/heating was demonstrated in the absence of the control streaks, which is in accordance with the linear-stability-theory for the still dominantly viscous instability. Then, the parametric study illustrated the control amplitude range in postponing the transition onset. It was revealed that amplitude- $(\rho u)'_{\max} / (\rho_\infty u_\infty)$ of 15.8–26.5%, 18–25.8%, and 20.8–25.2% are required for the cooled, adiabatic, and heated walls, respectively, to sustain a successful transition delay. It is therefore concluded that the accumulated influence of the control mode and the cooling increases the successful application range of the control amplitude, whereas the range is narrowed in the presence of weak heating.

Heating has no significant impact on the development of the control streaks, and the evolution of the disturbances in terms of their profile shape in the boundary layer. However, it strongly influences the growth rate of the disturbances, while dramatically reducing the application range of the

once-excited control streaks, i.e., low control amplitudes are not as effective as for the adiabatic or cooled cases. A second control strip, see Sharma *et al.* [21], might be useful for improving the effective use of the streaks. Besides, an alternative steady control mode (0,4) is also tested for the identical control amplitude range in adiabatic condition. It is found that the mode (0,4) with $(\rho u)'_{\max}/(\rho_{\infty} u_{\infty})$ of 16.8–24.1% is required to sustain a successful transition delay in the domain. Thereby, higher effectiveness of (0,5) was unveiled. It should be emphasized that the performed simulations in this study deal with a forced transition scenario at a single frequency and wave number, while transition control in a realistic scenario would be affected by the broadband freestream disturbances [7,12] and modified receptivity due to the introduction of the control devices [22,23].

For a comprehensive understanding of the effective applicability of the presented flow control mechanism, the research should be oriented to the investigation under strongly heated/cooled walls. To do so, LST must be exploited in order to estimate the most amplified frequency/wave number pair for each isothermal scenario. Besides, it is of our curiosity whether the control streaks might be used as an active control mechanism. Practical applications mostly require the adaption of a control system to the variations, slight or abrupt, in the environment. For that aim, a dynamic system should be implemented in the solver which serves as a bridge between the control strip and the downstream flow development. These two aspects would be significant extensions of the present work.

The data that support the findings of this study are available from the corresponding author upon reasonable request.

ACKNOWLEDGMENTS

The authors acknowledge the access to French HPC resources provided by the French regional computing center of Normandy (CRIANN) (Grants No. 1998022 and No. 2017002). M.C. appreciates the funding that is provided for his doctorate studies by the Region of Normandy, France.

-
- [1] M. M. Choudhari, F. Li, M. D. Bynum, M. A. Kegerise, and R. A. King, Computations of disturbance amplification behind isolated roughness elements and comparison with measurements, in *Proceedings of the 45th AIAA Fluid Dynamics Conference* (AIAA, Dallas, TX, 2015), p. 2625.
 - [2] A. Fedorov, Transition and stability of high-speed boundary layers, *Annu. Rev. Fluid Mech.* **43**, 79 (2011).
 - [3] P. S. Klebanoff, K. Tidstrom, and L. Sargent, The three-dimensional nature of boundary-layer instability, *J. Fluid Mech.* **12**, 1 (1962).
 - [4] T. Herbert, Secondary instability of boundary layers, *Annu. Rev. Fluid Mech.* **20**, 487 (1988).
 - [5] A. Thumm, Numerische Untersuchungen zum laminar-turbulenten Strömungsumschlag in transsonischen Grenzschichtströmungen, Ph.D. thesis, University of Stuttgart, 1991.
 - [6] H. Fasel, A. Thumm, and H. Bestek, Direct numerical simulation of transition in supersonic boundary layers: Oblique breakdown, in *Proceedings of the Fluids Engineering Conference* (ASME, New York, 1993), pp. 77–92.
 - [7] C.-L. Chang and M. R. Malik, Oblique-mode breakdown and secondary instability in supersonic boundary layers, *J. Fluid Mech.* **273**, 323 (1994).
 - [8] H. Bestek, A. Thumm, and M. Kloker, Realistic numerical simulation of boundary-layer transition experiments, in *Computational Fluid Dynamics* (John Wiley & Sons, New York, 1994), pp. 463–470.
 - [9] A. Fezer and M. Kloker, Spatial direct numerical simulation of transition phenomena in supersonic flat-plate boundary layers, in *Laminar-Turbulent Transition* (Springer, Berlin, 2000), pp. 415–420.
 - [10] F. Husmeier, C. Mayer, and H. Fasel, Investigation of transition of supersonic boundary layers at mach 3 using dns, in *Proceedings of the 43rd AIAA Aerospace Sciences Meeting and Exhibit* (AIAA, Reno, Nevada, 2005), p. 95.

- [11] C. S. Mayer, D. A. Von Terzi, and H. F. Fasel, Direct numerical simulation of complete transition to turbulence via oblique breakdown at mach 3, *J. Fluid Mech.* **674**, 5 (2011).
- [12] A. C. Laible and H. F. Fasel, Continuously forced transient growth in oblique breakdown for supersonic boundary layers, *J. Fluid Mech.* **804**, 323 (2016).
- [13] P. Wassermann and M. Kloker, Mechanisms and passive control of crossflow-vortex-induced transition in a three-dimensional boundary layer, *J. Fluid Mech.* **456**, 49 (2002).
- [14] C. Cossu and L. Brandt, Stabilization of tollmien–schlichting waves by finite amplitude optimal streaks in the blasius boundary layer, *Phys. Fluids* **14**, L57 (2002).
- [15] J. H. Fransson, L. Brandt, A. Talamelli, and C. Cossu, Experimental study of the stabilization of tollmien–schlichting waves by finite amplitude streaks, *Phys. Fluids* **17**, 054110 (2005).
- [16] J. H. M. Fransson, A. Talamelli, L. Brandt, and C. Cossu, Delaying Transition to Turbulence by a Passive Mechanism, *Phys. Rev. Lett.* **96**, 064501 (2006).
- [17] S. Bagheri and A. Hanifi, The stabilizing effect of streaks on tollmien-schlichting and oblique waves: A parametric study, *Phys. Fluids* **19**, 078103 (2007).
- [18] S. Shahinfar, S. S. Sattarzadeh, J. H. M. Fransson, and A. Talamelli, Revival of Classical Vortex Generators Now for Transition Delay, *Phys. Rev. Lett.* **109**, 074501 (2012).
- [19] P. C. Dörr and M. J. Kloker, Numerical investigations on tollmien–schlichting wave attenuation using plasma-actuator vortex generators, *AIAA J.* **56**, 1305 (2018).
- [20] P. Paredes, M. M. Choudhari, and F. Li, Instability wave-streak interactions in a supersonic boundary layer, *J. Fluid Mech.* **831**, 524 (2017).
- [21] S. Sharma, M. S. Shadloo, A. Hadjadj, and M. J. Kloker, Control of oblique-type breakdown in a supersonic boundary layer employing streaks, *J. Fluid Mech.* **873**, 1072 (2019).
- [22] S. Kneer, Z. Guo, and M. J. Kloker, Control of laminar breakdown in a supersonic boundary layer employing streaks, *J. Fluid Mech.* **932**, A53 (2022).
- [23] S. Kneer, Control of laminar breakdown in a supersonic boundary layer employing streaks, Master’s thesis, Institute of Aerodynamics and Gas Dynamics, University of Stuttgart, 2020.
- [24] A. Wazzan and H. Taghavi, The effect of heat transfer on three-dimensional spatial stability and transition of flat plate boundary layer at mach 3, *Int. J. Heat Mass Transf.* **25**, 1321 (1982).
- [25] V. I. Lysenko and A. A. Maslov, The effect of cooling on supersonic boundary-layer stability, *J. Fluid Mech.* **147**, 39 (1984).
- [26] S. Sharma, Laminar-to-turbulent transition in supersonic boundary layer: Different scenarios and possible control, Ph.D. thesis, Normandie Université, 2019.
- [27] M. Shadloo, A. Hadjadj, and F. Hussain, Statistical behavior of supersonic turbulent boundary layers with heat transfer at $m_\infty = 2$, *Int. J. Heat Fluid Flow* **53**, 113 (2015).
- [28] M. Kloker, Direkte numerische Simulation des laminar-turbulenten Strömungsumschlages in einer stark verzögerten Grenzschicht, Ph.D. thesis, Fakultät Verfahrenstechnik Universität Stuttgart, 1993.
- [29] F. M. White and I. Corfield, *Viscous Fluid Flow*, Vol. 3 (McGraw–Hill New York, 2006).
- [30] M. Shadloo and A. Hadjadj, Laminar-turbulent transition in supersonic boundary layers with surface heat transfer: A numerical study, *Numer. Heat Transf. A* **72**, 40 (2017).
- [31] J. L. Potter, Review of the influence of cooled walls on boundary-layer transition, *AIAA J.* **18**, 1010 (1980).
- [32] I. Lienhard and H. John, *A Heat Transfer Textbook* (Phlogiston Press, Cambridge, Massachusetts, 2005).
- [33] H. Schlichting and K. Gersten, *Boundary-layer Theory* (Springer, Berlin, 2016).
- [34] T. C. J. Cousteix, *Modeling and Computation of Boundary-layer Flows* (Springer, Berlin, 2005).
- [35] J. Crouch, Receptivity issues for laminar-flow control, in *Proceedings of the IUTAM Symposium on Mechanics of Passive and Active Flow Control* (Springer, Berlin, 1999), pp. 151–158.
- [36] J. C. R. Hunt, A. A. Wray, and P. Moin, Eddies, stream, and convergence zones in turbulent flows, in *Proceedings of the Summer Program* (Center for Turbulence Research, Stanford, 1988).
- [37] P. Paredes, M. M. Choudhari, and F. Li, Nonlinear transient growth and boundary layer transition, in *Proceedings of the 46th AIAA Fluid Dynamics Conference* (AIAA, Washington, D.C., 2016), p. 3956.
- [38] P. Paredes, M. M. Choudhari, and F. Li, Transition due to streamwise streaks in a supersonic flat plate boundary layer, *Phys. Rev. Fluids* **1**, 083601 (2016).